Bose-Einstein Condensates with Spin-Orbit Interaction

Tin-Lun Ho and Shizhong Zhang

Phys. Rev. Lett. **107**, 150403 — Published 6 October 2011

DOI: 10.1103/PhysRevLett.107.150403

Bose-Einstein Condensates with Spin-Orbit Interaction

Tin-Lun Ho and Shizhong Zhang
Department of Physics, The Ohio State University, Columbus, OH 43210

Motivated by recent experiments carried out by Spielman's group at NIST [1, 2], we study a general scheme for generating families of gauge fields, spanning the scalar, spin-orbit, and non-abelian regimes. The NIST experiments, which impart momentum to bosons while changing their spin state, can in principle realize all these. In the spin-orbit regime, we show that a Bose gas is a spinor condensate made up of two non-orthogonal dressed spin states carrying different momenta. As a result, its density shows a stripe structure with a contrast proportional to the overlap of the dressed states, which can be made very pronounced by adjusting the experimental parameters.

The recent success of the NIST group [1, 2] in generating abelian gauge fields in ultracold atomic gases has created exciting opportunities to simulate electronic transport in solids using these highly configurable gases. Recently, the NIST group has also reported the creation of spin-orbit coupling in a pseudo spin-$\frac{1}{2}$ Bose gas [3]. This is a significant development in cold atom research. Not only will this allow for the simulation of a wide array of spin-orbit effects in solids, it will also provide opportunities to study spin-orbit effects in bosons, giving rise to a class of quantum many-body effects with no analog in solids.

What is amazing is the simplicity of the experimental setup. The key element consists of only a pair of lasers and an external magnetic field. Moreover, going from the previously studied abelian gauge fields [1, 2] to the spin-orbit case [3] (as well as the non-abelian regime) requires nothing more than turning down the laser power, showing that all these regimes are continuously connected to each other. In this paper, we show that in the presence of spin-orbit interaction, and more generally in the presence of non-abelian gauge fields [4–18], a spinor condensate will develop a spontaneous stripe structure in each spin component, reflecting a ground state made up of two non-orthogonal dressed states with different momenta. Depending on interactions, this ground state can reduce to a single dressed state. These momentum-carrying stripes are the *macroscopic* bosonic counterpart of the spin-orbit phenomena in fermions that are being actively studied in electron physics today.

Since spin-orbit interactions are closely related to non-abelian gauge fields, we shall first discuss a general scheme for creating effective gauge fields that allow one to go continuously from the abelian to spin-orbit, to non-abelian regimes. We shall refer to this as the "generalized adiabatic" scheme. It works as follows: consider the hamiltonian $h = \mathbf{p}^2/2M + W(\mathbf{r})$ that operates on an atom with internal degrees of freedom, such as alkali atoms with hyperfine spin F. W is a potential in spin space that varies spatially with characteristic wave-vector q. The energy scale for the spatial variation of W is then $\epsilon_q = \hbar^2 q^2/2M$. If W has a group of L states ($L < 2F + 1$) at the bottom of its spectrum lying within an energy range $\Delta E \ll \epsilon_q$ and is well separated from all other higher energy spin states by ϵ_q, then the low energy phenomena of the system can be described within this reduced manifold of L states. By going into a frame in this manifold that transforms away the spatial variations of the spin states, a gauge field emerges [19, 20]. The gauge field is abelian if $L = 1$. For $L \geq 2$, a spin-orbit interaction or non-abelian gauge field can emerge. Thus, by moving the high energy states across ϵ_q into the low energy manifold, one can increase the dimensionality of this low energy manifold and create non-abelian gauge fields with increasingly rich structure. It should be noted that this is very different from the tripod scheme in most theoretical proposals, which makes use of a set of dark states sitting above a short-lived ground state of the system [5]. In contrast, the generalized adiabatic scheme uses the lowest energy states, thereby eliminating collisional loss and hence, the intrinsic heating of the tripod scheme.

Before proceeding, it is useful to note the unique features of non-abelian gauge fields. In the abelian case, a *constant* vector potential has no physical effect since it can be gauged away. This is not true for the non-abelian case, however, because of its non-commutativity and a constant non-abelian vector potential will give rise to physical effects. Moreover, non-abelian gauge fields inevitably lead to spin-orbit coupling, so any potential (such as a confining trap) that alters particle trajectories also causes spin rotation. This immediately implies significant differences between bosons and fermions. For fermions, the Pauli principle means that any spin effects are the result of contributions from all occupied states. In contrast, bosons will search for or even construct (through interaction effects) an optimum (i.e., lowest energy) spin state which will become macroscopically occupied at low temperatures thanks to Bose statistics. This Bose enhancement gives rise to gauge field effects *visible at the macroscopic level.* The current experiments at NIST already give a way to study macroscopic spin-orbit effects.

(A) The NIST setup and the effective hamiltonian: The NIST setup consists of two counter propagating lasers with frequency difference ω and momentum

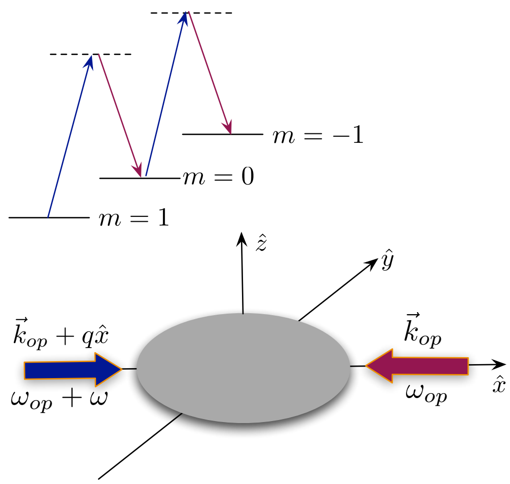

FIG. 1. Schematic of the experimental setup at NIST [3]. The Raman process consists of two lasers with wave vectors $\mathbf{k}_{op}+q\hat{x}$ and $\mathbf{k}_{op}$, frequencies $\omega_{op}+\omega$ and ω_{op} impinging on the atomic cloud. Atoms excited by the laser will have their momenta increased by $q\hat{x}$ while their spin projection along $\hat{\mathbf{y}}$ is changed by 1, as shown in the energy diagram at top.

difference q directed along $\hat{\mathbf{x}}$ impinging on a spin $F=1$ Bose condensate of ^{87}Rb atoms. There is also a magnetic field along $\hat{\mathbf{y}}$ with a field gradient. (See Figure 1). The lasers induces a Raman transition in the atom, transferring linear momentum $q\hat{\mathbf{x}}$ to the Bose gas while increasing the spin angular momentum by $\hbar$ at the same time. A similar scheme has been proposed earlier in Ref.[21]. The single particle hamiltonian is $h(t)=\frac{\mathbf{p}^2}{2M}+W(t)$, where $W(t)=-\hbar\Omega_y F_y+\hbar\lambda F_y^2-\frac{\hbar\Omega_R}{2}[e^{i(qx-\omega t)}(F_z+iF_x)+h.c.]$, where $\mathbf{F}$ is the spin-1 operator. $\hbar\lambda$ is the quadratic Zeeman energy. $\hbar\Omega_y=\hbar\Omega_o+Gy$ is the Zeeman energy produce by the magnetic field along $\hat{\mathbf{y}}$. The Ω_o term is due to the constant magnetic field and the Gy term comes from the field gradient. Ω_R is the Rabi frequency associated with the Raman process. In the frame rotating in spin space about $\hat{y}$ with frequency ω, the hamiltonian becomes static, $H=h(t=0)+\hbar\omega F_z$, and is given by $H=\frac{\mathbf{p}^2}{2M}+W$, with

$$W/\hbar=-\overline{\Omega}_y F_y+\lambda F_y^2-\Omega_R(\mathrm{cos}qxF_z-\mathrm{sin}qxF_x) \quad (1)$$

$$=e^{-iqxF_y}\left(-\overline{\Omega}_y F_y+\lambda F_y^2-\Omega_R F_z\right)e^{iqxF_y} \quad (2)$$

and $\overline{\Omega}_y=\Omega_o-\omega+Gy$.

Eq.(2) shows that W has a very simple level structure in the frame rotating in spin space along $\hat{\mathbf{y}}$ with angle qx. For simplicity, we take $F=1$ and $G=0$. The following cases are of particular interest:

(i) Abelian case: this occurs when $\Omega_R\gg\lambda,\epsilon_q/\hbar$, with ω tuned close to Ω_o so that $\overline{\Omega}_y\sim 0$. The ground state in the rotating frame is the $m=+1$ state along $\hat{\mathbf{z}}$, isolated from the other two states ($m=0,-1$ along $\hat{\mathbf{z}}$) by $\sim\hbar\Omega_R>\epsilon_q$.

(ii) Spin-orbit case: this occurs when $\lambda\gg\Omega_R,\epsilon_q$, with ω tuned closed to $\omega=\Omega_o-\lambda$. In this case, the states $m=1$ and $m=0$ along $\hat{\mathbf{y}}$ lie at the bottom of the spectrum, separated from the third state $m=-1$ by $2\hbar\lambda>\epsilon_q$. We shall from now on focus on this case.

Let $\hat{\psi}^\dagger_m$ and $\hat{\phi}^\dagger_m$ be the operators that create a boson with spin projection m along $\hat{\mathbf{y}}$ in the laboratory frame and in the rotating frame in spin space; and $\hat{\psi}_m=\left(e^{iqxF_y}\hat{\phi}\right)_m=e^{iqxm}\hat{\phi}_m$. Focusing on the lowest two states $\hat{\phi}_m$, $m=1,0$, the hamiltonian is

$$\hat{\mathcal{K}}=\int\left[\hat{\phi}^\dagger_m H_{mn}\hat{\phi}_n+\frac{1}{2}\hat{n}_m g_{mn}\hat{n}_n-(V-\mu)\hat{n}\right] \quad (3)$$

where $\hat{n}_m=\hat{\phi}^\dagger_m\hat{\phi}_m$, $\hat{n}=\sum_m\hat{n}_m$, $V=\frac{1}{2}M\omega_T^2\mathbf{r}^2$ is the harmonic trap, μ is the chemical potential, g_{mn} are interactions between bosons in spin states m and n, $g_{10}=g_{01}$, and

$$H_{mn}=\frac{\hbar^2}{2M}\left[\frac{\nabla}{i}+\hat{\mathbf{x}}q\begin{pmatrix}1&0\\0&0\end{pmatrix}\right]^2+\hbar\begin{pmatrix}-Gy&\frac{\Omega_R}{\sqrt{2}}\\\frac{\Omega_R}{\sqrt{2}}&0\end{pmatrix}. \quad (4)$$

When $G=0$, the solutions χ of the resulting Schrödinger equation

$$H_{mn}(x)\chi_n(x)=E\chi_m(x) \quad (5)$$

have the following property that

$$\chi'_m(x)=e^{i\gamma}e^{-iqx}(\tau_1)_{mn}\chi^*_n(x),\quad \tau_1=\begin{pmatrix}0&1\\1&0\end{pmatrix} \quad (6)$$

is also a solution, where γ is an arbitrary phase.

(B) Single particle ground state: for zero-field gradient, $G=0$, the momentum eigenstates are of the form $\chi^{(p)}_m(x)=e^{ipx}\widetilde{\chi}_m$, $\widetilde{\chi}\equiv\binom{u}{v}$, and Eq.(5) becomes

$$\frac{\hbar^2}{M}\left(\frac{k^2+Q^2}{2}+kQ\tau_2+\ell^2\tau_1\right)\begin{pmatrix}u\\v\end{pmatrix}=E_p\begin{pmatrix}u\\v\end{pmatrix}, \quad (7)$$

where we have defined

$$Q\equiv q/2,\qquad k\equiv p+Q. \quad (8)$$

and, for later use, have expressed $\hbar\Omega_R$ in terms of the wave-vector ℓ and angle θ:

$$\frac{\ell^2}{Q^2}\equiv\frac{M\Omega_R}{\hbar\sqrt{2}Q^2}=\frac{\sqrt{2}\hbar\Omega_R}{\epsilon_q}\equiv\mathrm{sin}\theta. \quad (9)$$

The eigenvalues come in two branches, with energies $E_{1(0)}(p)=\frac{\hbar^2}{M}\left(\frac{k^2+Q^2}{2}+(-)\sqrt{(kQ)^2+\ell^4}\right)$(see Fig. 2). The ground states are the minima of $E_0(p)$ at

$$p_\pm=\pm k_o-q/2,\qquad k_o=\sqrt{Q^2-\ell^4/Q^2}=(q/2)\mathrm{cos}\theta, \quad (10)$$

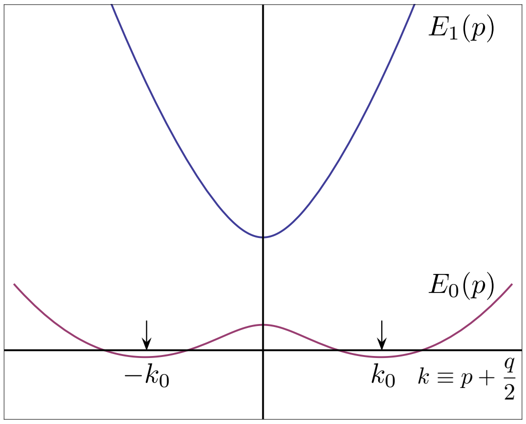

FIG. 2. The energy levels $E_0(p)$ and $E_1(p)$ as a function of $k \equiv p + q/2$. The lower branch $E_0(p)$ has two degenerate minima at $k = \pm k_0$, where $k_0 = (q/2)\cos\theta$. The energy difference between the lower and upper branch at $\pm k_0$ is $\epsilon_q = \hbar^2 q^2/2m$.

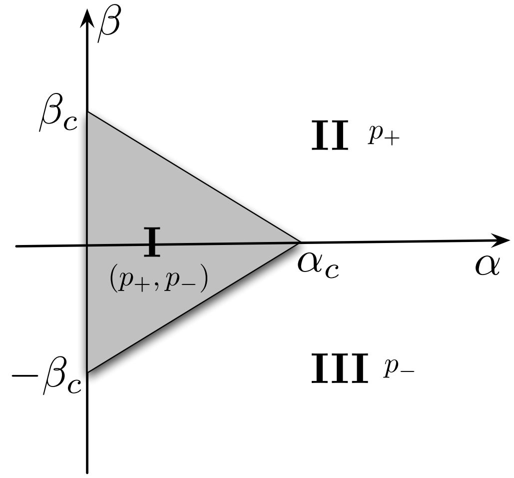

FIG. 3. The phase diagram of pseudo spin 1/2 Bose gas: Region **I** is a superposition of two dressed state with momentum p_+ and p_-, **II** and **III** are the single dressed states p_+ and p_- respectively. α, β, α_c, and β_c are defined in text.

with energy

$$E_0(p_\pm) = -\frac{\hbar^2 \ell^4}{2MQ^2} = -\frac{1}{2}\frac{(\hbar\Omega_R)^2}{\epsilon_q} \equiv E_o. \quad (11)$$

The energy of the upper branch at these momenta is $E_1(p_\pm) = \epsilon_q - \hbar^2\ell^4/(2MQ^2)$, which is higher by ϵ_q. It is worth noting that the value of the ground state energy is not of the order $-\hbar\Omega_R$, but a higher energy $-(\hbar\Omega_R)^2/\epsilon_q$. The wavefunctions at these degenerate ground states are $\chi_m^{(p_\pm)}(x) = e^{ip_\pm x}\widetilde{\chi}_m^{(p_\pm)}$,

$$\widetilde{\chi}^{(p_+)} = \begin{pmatrix} i\sin\frac{\theta}{2} \\ \cos\frac{\theta}{2} \end{pmatrix}, \ \widetilde{\chi}^{(p_-)} = \begin{pmatrix} i\cos\frac{\theta}{2} \\ \sin\frac{\theta}{2} \end{pmatrix}. \quad (12)$$

Note that the states $\chi^{(p_\pm)}(x)$ are connected by Eq.(6) with $\gamma = \pi/2$. They are orthogonal due to their different momenta. The spin states, however, have non-zero overlap, since

$$\langle p_+|p_-\rangle = \widetilde{\chi}^{(p_+)\dagger}\widetilde{\chi}^{(p_-)} = \sin\theta. \quad (13)$$

(C) Pseudo spin-1/2 spinor condensate: condensing in the dressed states $|p^{(\pm)}\rangle$, the field operator, which admits the expansion $\hat{\phi}_m(x) = \sum_p \chi_m^{(p)}(x)\hat{a}_p$, turns into a spinor field of the form

$$\Phi_m(x) = A_+\chi_m^{(p_+)}(x) + A_-\chi_m^{(p_-)}(x). \quad (14)$$

Because of the non-zero overlap, Eq.(13), the density $n_m(x) = |\Phi_m(x)|^2$ of each spin component will develop a stripe structure. This can be seen by noting that the total density $n(x) = n_1(x) + n_0(x)$ and the "magnetization" $m(x) = n_1(x) - n_0(x)$ are given by

$$n(x) = |A_+|^2 + |A_-|^2 + \sin\theta(A_+^* A_- e^{-2ik_o x} + c.c.) \quad (15)$$

$$m(x) = -\cos\theta(|A_+|^2 - |A_-|^2). \quad (16)$$

Note also that $m(x)$ is independent of θ. Eq.(15) shows that the contrast of the oscillation is set by the overlap, $\sin\theta$, whereas the wavelength of the stripe is $\pi/k_o = 2\pi/(q\cos\theta)$. Thus, both contrast and wavelength increase with θ for $\theta < \pi/2$.

The amplitudes $A_\pm$ are determined by minimizing the Gross-Pitaevskii (GP) functional of Eq.(3), which is obtained by replacing $\hat{\phi}_m(x)$ with the c-number $\Phi_m(x)$, and $\hat{n}_m(x)$ with $n_m(x) = |\Phi_m(x)|^2$. Defining $|\mathbf{A}|^2 = |A_+|^2 + |A_-|^2$, and $a_\pm \equiv A_\pm/|\mathbf{A}|$, the GP functional then reads,

$$\mathcal{K} = (E_o - \mu)|\mathbf{A}|^2 + \frac{1}{2}|\mathbf{A}|^4 G(a_+, a_-), \quad (17)$$

where $|\mathbf{A}|^4 G(a_+, a_-) = \int g_{mn} n_m(x) n_n(x)$. Note that while A_+ and A_- give distinct contributions to the kinetic energy due to their differing momenta $p_\pm$, they are coupled through interaction due to the overlap of their spin functions. For example, $\int n_1^2(x) = \int[n^2(x) + m^2(x) + 2n(x)m(x)]/4$, and the mixing of A_+ and A_- appears in $\int n^2(x)$. To minimize $\mathcal{K}$, we first minimize $G(a_+, a_-)$ with the constraint $|a_+|^2 + |a_-|^2 = 1$ to obtain the optimal value (a_+^o, a_-^o) and

$$|\mathbf{A}|^2 = (\mu - E_o)/G_o, \quad G_o = G(a_+^o, a_-^o). \quad (18)$$

Since the minimization is straightforward, we shall only present the results, which are shown in Fig. 3. The phase diagram depends on the parameters

$$\alpha = g_{10}/g, \quad \beta = (g_{11} - g_{00})/g, \quad g = (g_{11} + g_{00})/2. \quad (19)$$

and two numbers α_c and β_c derived from the laser parameter $\sin\theta$ defined in Eq.(9). They are $\alpha_c \equiv \frac{2-\tan^2\theta}{2+\tan^2\theta}$, and $\beta_c = \cos\theta(2 - \tan^2\theta)$. For $g_{11}, g_{00}, g_{10} > 0$, (as in ^{87}Rb), there are three possibilities: (**I**) Two dressed states, with both $A_\pm \neq 0$; single dressed state with (**II**) $\chi_{p_+}(x)$, $(A_- = 0)$, or (**III**) $\chi_{p_-}(x)$, $(A_+ = 0)$.

Phase (**I**) occurs within the triangle shown in Fig.3, bounded by the lines $xy_c \pm yx_c = x_c y_c$. The region exists only when $\alpha_c > 0$, which means $\sin\theta < \sqrt{2/3}$. Otherwise, interaction effect will drive the condensate into a single dressed state. In phase (**I**), the amplitudes are

$$|a^o_\pm|^2 = \frac{1}{2}\left(1 \pm \frac{\beta/\cos\theta}{2 - 2\alpha - (1+\alpha)\tan^2\theta}\right), \tag{20}$$

and $G_o = G(a^o_+, a^o_+) = -\frac{\beta^2}{2(2-2\alpha-(1+\alpha)\tan^2\theta)} + (1+\alpha)(1+\frac{1}{2}\sin^2\theta)$. The relative phase between A_+ and A_-, however, cannot be determined within the GP approach. This phase can be fixed by perturbations such as field gradient the breaks the symmetry Eq.(6), or by quantum fluctuation effects that go beyond GP. As discussed before, the density of each of the spin component n_1 and n_0 of this phase has a stripe structure. The case $\beta = 0$ $(g_{11} = g_{00})$ is special. In that case, we have $|A_+| = |A_-|$ for $\alpha < \alpha_c$. For $\alpha > \alpha_c$, the two dressed states $\chi^{(p_+)}$ and $\chi^{(p-)}$ are degenerate.

In the presence of a harmonic trap $V(\mathbf{r}) = \frac{1}{2}M\omega_T^2\mathbf{r}^2$ with harmonic length $d = \sqrt{\hbar/(M\omega)} \gg 2\pi/q$, the wavelength of the stripe, we can apply Thomas-Fermi approximation, and the condensate wavefunction is given by Eq.(14), (18) and (20) with chemical potential μ in Eq.(18) replaced by $\mu(\mathbf{r}) = \mu - V(\mathbf{r})$, i.e. for Phase **(I)**,

$$\Phi_m = \sqrt{\tfrac{\mu(\mathbf{r})-E_o}{G_o}}[a^o_+ e^{ip_+x}\begin{pmatrix} i\sin\frac{\theta}{2} \\ \cos\frac{\theta}{2}\end{pmatrix} + e^{i\gamma}a^o_- e^{ip_-x}\begin{pmatrix} i\cos\frac{\theta}{2} \\ \sin\frac{\theta}{2}\end{pmatrix}] \tag{21}$$

The density profile $n_1(\mathbf{r})$ for the $m = 1$ spin component along $\hat{\mathbf{y}}$ is shown in Fig. 4 for e.g., $\theta = \frac{1}{4}\pi$, $N = 2.5\times 10^5$.

Apart from the stripe structure, the presence of these phases can be detected by measuring the displacement of the atom cloud after expansion when the trap is turned off. For the condensate with two dressed states, after expansion, the cloud will separate into two atom clouds moving with different momenta. In contrast, for the condensate in a single dressed state, the cloud will expand in one direction, depending on the momentum $p_\pm$.

T.L. Ho would like thank Ian Spielman for discussions of his experiments. This work is supported by NSF Grant DMR-0907366 and by DARPA under the Army Research Office Grant Nos. W911NF-07-1-0464, W911NF0710576.

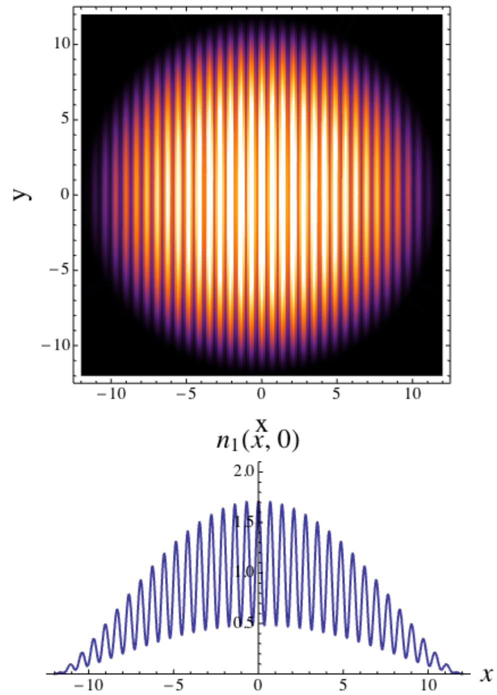

FIG. 4. The upper figure is the column density $\widetilde{n}_1(x,y) = \int dz n_1(x,y,z)$. The lower frame is $\widetilde{n}_1(x,0)$. The period of oscillation is π/k_o. The contrast of oscillation at the center is 70%. Our calculation is performed for ^{87}Rb with $N = 2.5\times 10^5$ atoms, $q = 1.56\times 10^7 m^{-1}$, $\theta = \frac{1}{4}\pi$, $\hbar\Omega_R = h\times 7.1$KHz, cloud size $R_{TF} = 20\mu$m[1]. The values α and β used are given by $\alpha = \frac{1}{4}\alpha_c$ and $\beta = \frac{1}{4}\beta_c$. The length displayed is in units of the laser wavelength $804.3nm$ in ref.[1] .

[1] Lin,Y.-J., Compton, R. L., Perry,A.R., Phillips,W.D., Porto,J.V., and Spielman,I.B. Phys.Rev.Lett. **102**, 130401 (2009)
[2] Lin,Y.-J., Compton, R. L., Jimnez-Garca,K., Porto, J.V., and Spielman, I. B. Nature, **462**, 628-632 (2009)
[3] Lin,Y.-J., Jimnez-Garca,K. and Spielman, I. B. Nature, **471**, 83-86 (2011)
[4] Osterloh,K., Baig,M.,Santos,L., Zoller,P., and Lewenstein,M. Phys.Rev.Lett. **95**, 010403 (2005)
[5] Ruseckas,J., Juzeliūnas,G., Öhberg,P. &Fleischhauer, M. Phys.Rev.Lett. **95**,010404 (2005)
[6] Vaishnav,J.Y., and Clark, C.W. Phys.Rev.Lett. **100**, 153002 (2008)
[7] Satija, I.I., Dakin, D.C., Vaishnav J.Y. and Clark,C.W. Phys. Rev. A **77**, 043410 (2008)
[8] Satija, I.I., Dakin, D.C. and Clark,C.W. Phys. Rev. Lett **97**, 216401 (2006)
[9] Juzeliūnas,G.,Ruseckas,J., Jacob,A., Santos,L., and Öhberg,P. Phys.Rev.Lett. **100**, 200405 (2008)
[10] Merkl,M., Juzeliūnas,G., and Öhberg,P. Eur.Phys.J.D. **59**, 257 (2010)
[11] Goldman,G., Kubasiak, A., Gaspard, P., and Lewenstein,M. Phys.Rev.A **79**, 023624 (2009)
[12] Goldman,G., Kubasiak, A., Bermudez, A., Gaspard, P., and Lewenstein,M. Phys.Rev.Lett. **103**, 035301 (2009)
[13] Wang, C.J., Gao, C., Jian, C.M., and Zhai, H. Phys.Rev.Lett. **105**, 160403 (2010)
[14] Wu, C.J. and Mondragon-Shem, I. arXiv:0809.3532v3

[15] Stanescu T., Anderson B., and Galitski V. Phys.Rev.A **78**, 023616 (2008)
[16] Larson J. and Sjoqvist E. Phys.Rev.A **79**, 043627 (2009)
[17] Yip. S.-K., Phys.Rev.A **83**, 043616 (2011)
[18] Gerbier,F. and Dalibard,J. New Journal of Physics, **12**, 033007 (2010)
[19] Wilczek,F. and Zee,A. Phys.Rev.Lett. **52**, 2111 (1984)
[20] S. Ulreich and W. Zwerger, Euro. Lett. **41**, 117 (1998)
[21] Higbie, J. and Stamper-Kurn, D.M. Phys.Rev.Lett. **88**,090401 (2002)